Electron energy transport in the presence of rational surfaces in the Wendelstein 7-AS stellarator

2002 Nucl. Fusion 42 903

(http://iopscience.iop.org/0029-5515/42/7/313)

INSTITUTE OF PHYSICS PUBLISHING and INTERNATIONAL ATOMIC ENERGY AGENCY NUCLEAR FUSION

Nucl. Fusion **42** (2002) 903–912 PII: S0029-5515(02)37941-9

Electron energy transport in the presence of rational surfaces in the Wendelstein 7-AS stellarator

R. Brakel and W7-AS Team

Max-Planck-Institut für Plasmaphysik, Euratom Association, Garching, Germany

E-mail: brakel@ipp.mpg.de

Received 2 August 2001, accepted for publication 12 November 2001
Published 18 July 2002
Online at stacks.iop.org/NF/42/903

Abstract

Electron energy transport in the Wendelstein 7-AS stellarator exhibits a strong sensitivity to the boundary value of the rotational transform when the magnetic shear is low. Pronounced confinement maxima close to the low order rational ι values correlate with a low density of other rational numbers in these favourable ι ranges. The ι dependence is lost if magnetic shear is increased by large plasma currents. The hypothesis is proposed that, at rational flux surfaces, electron energy transport is increased above the already anomalous level and that magnetic shear reduces the additional enhancement. An empirical model that incorporates these features into a simple expression for the electron heat conductivity can reproduce the experimental dependences over a wide range of external control parameters, e.g. the rotational transform and the net plasma current. Except for the explicit shear dependence, this model bears a remarkable similarity to the RTP model, which successfully describes the electron transport barriers near low order rational q surfaces in RTP and other tokamaks.

PACS numbers: 52.55.Hc, 52.25.Fi

1. Introduction

Except for the long mean free path regime with very low collisionality, electron energy transport in stellarators appears, as in tokamaks, to be anomalously enhanced as compared with the neoclassical prediction. It is common opinion that anomalous transport originates from plasma turbulence, but its nature has not yet been resolved. Electrostatic turbulence is the most likely candidate, but magnetic turbulence cannot be ruled out. In parallel to pushing forward the theories of turbulent transport, systematic experiments are required to reveal the dependences of anomalous transport on the experimental control parameters. The Wendelstein 7-AS (W7-AS) stellarator [1] is ideally suited to studying the effect of the rotational transform ι and the magnetic shear, $\iota' = d\iota/dr$, on anomalous electron transport. With selective electron heating by ECRH and, at appropriate plasma density, low collisional energy transfer to the ions, the electrons are energetically decoupled from the ions. Furthermore, Wendelstein stellarators have very low magnetic shear in the vacuum field and the value of ι can be varied widely in W7-AS. The low shear design allows avoidance of the major rational ι values in the confinement volume which might otherwise resonate with magnetic field perturbations and cause the formation of magnetic islands. Additionally, the low shear design offers the experimental flexibility to control the magnetic shear in a finite pressure plasma by externally (inductively [2], electron cyclotron resonance [3] or neutral beam [4]) driven plasma currents. Since in a stellarator a toroidal net current is not required for confinement, the magnitude and direction of the current and thus the size and sign of the magnetic shear can be freely chosen.

A strong impact of the ι value and the magnetic shear on plasma confinement was previously observed in the W II-A and W VII-A [5] stellarators, and it appears in W7-AS as well [2, 6]. With small shear, optimum confinement is found in narrow operation windows in the direct vicinity of the low order rational values $\iota = 1/2, 1/3$, etc, indicating that electron transport is smaller when ι is close to (but not identical with) these particular values than otherwise. The immediate neighbourhood of low order rational numbers is characterized by a lower density of higher order rational numbers, except those of very high order [7]. It has therefore been assumed that perturbations arising at higher order rational surfaces enhance the electron transport. Such perturbations may be static and inherent to the confining magnetic field [7], or they may be dynamic, arising, for example, from turbulence or MHD activity [2]. The strong dependence of confinement on the value of ι is mitigated by increasing the magnetic shear, either by external current drive [2] or by pressure induced currents [8].

It is very remarkable that local features in the electron temperature profiles of various tokamaks (e.g. RTP [9], JET [10] and TEXTOR-94 [11]) are also strictly correlated with the occurrence of low order rational $\iota(=1/q)$ values. In line with the observations at W7-AS, a strong reduction of electron heat transport can arise close to these values. Because of the shear, which is inherent to tokamaks, this reduction is radially localized, giving rise to electron transport barriers, which have been detected by means of high resolution electron temperature diagnostics. It may be conjectured that the relations which obviously exist between anomalous electron transport and the occurrence of low order rational ι values are governed by the same physics in both stellarators and tokamaks.

This article reports on the experimental and modelling efforts at W7-AS to obtain greater insight into the sensitive dependence of electron energy transport on rotational transform and magnetic shear. In section 2 an overview is given of the vacuum field properties of W7-AS and of the impact of pressure and externally driven currents on the ι profile. Section 3 summarizes the results from ECRH discharges with inductive net current control. In these experiments the boundary value of ι and the plasma current are systematically varied to change both the absolute value of ι and the magnetic shear. From the experimental results an empirical model for the electron heat conductivity has been developed which is introduced in section 4. The model explicitly relates anomalous transport to the occurrence of rational surfaces and to the magnetic shear. Results from the model are compared with the experiment in section 5. A confinement bifurcation predicted by the model for the case where the plasma current is allowed to evolve freely was demonstrated experimentally. The results are discussed in section 6.

2. Experimental conditions

In W7-AS (major radius $R = 2\,\mathrm{m}$, minor radius $a \leqslant 0.18\,\mathrm{m}$, magnetic field $B_0 \leqslant 3\,\mathrm{T}$) the value of the external rotational transform ι_{ex} can be varied from 0.25 to 0.7. The magnetic shear in the vacuum field is very small, being slightly negative for $\iota_{ex,a} < 0.4$ and slightly positive for $\iota_{ex,a} > 0.4$ (figure 1(a)), where $\iota_{ex,a}$ is the value of ι_{ex} at the boundary. W7-AS is equipped with a transformer for inductive current drive. The fivefold toroidal periodicity gives rise to 'natural' $5/m$ perturbation components in the Fourier spectrum of the magnetic field. Additional $1/2$ and $1/3$ perturbations exist owing to field errors. The detailed flux surface mapping of the vacuum field [6] has confirmed both the existence of closed nested surfaces if these major resonances are excluded, e.g. for $\iota_{ex,a} = 0.48$, and the existence of magnetic islands if the ι profile contains such resonances, e.g. $1/2 = 5/10$ for $\iota_{ex,a} = 0.51$. When located at the edge, the vacuum field islands considerably reduce the effective minor radius a since their size becomes large owing to the small shear. According to the empirical a^2 dependence of the international stellarator scaling ISS95 [12], this causes an inherent ι dependence of confinement in W7-AS if the full available plasma aperture is used and shear is small. When the islands move radially inward during a variation of ι, their width, $w_{mn} \sim B_{mn}^{1/2}$, decreases since the perturbation amplitudes $B_{mn} \sim r^{m-1}$ rapidly decrease towards the magnetic axis. Therefore in most of the experiments reported here the plasma aperture has been reduced by means of the two vertically movable rail limiters in order to weaken the effect of boundary islands. This should also quench the unintended occurrence of the H mode, which is strongly related to the $5/m$ boundary islands [13]. Indeed, there is no experimental evidence of the H mode for the discharges under discussion. Additionally, a recently installed set of two control coils per toroidal field period can be used to vary the size of the $5/m$ islands, including their full compensation [14].

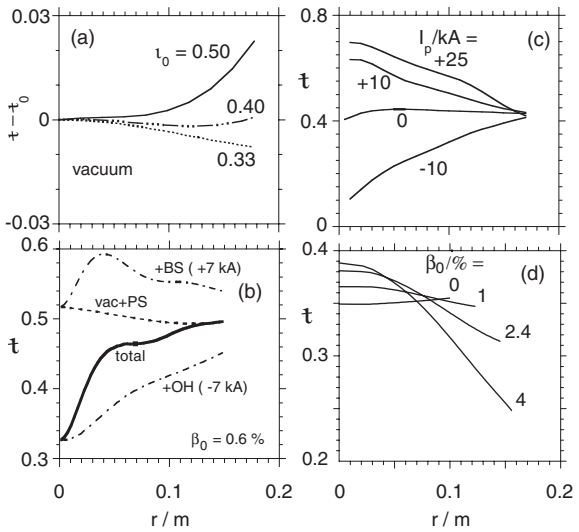

Figure 1. Radial profiles of the rotational transform in W7-AS: (a) in the vacuum field for different central values of ι_0; (b) in a net current free ECRH discharge with contributions from the vacuum field (vac), Pfirsch–Schlüter (PS), bootstrap (BS) and inductive (OH) currents; (c) in ECRH discharges with inductively driven net currents I_p; and (d) in neutral beam heated discharges at high β.

At finite plasma pressure p the bootstrap current, the Pfirsch–Schlüter (PS) equilibrium current and, optionally, externally driven currents modify the field structure. The bootstrap current in W7-AS increases the rotational transform. The PS current increases ι in the centre and decreases ι at the edge. The current distribution cannot be measured in W7-AS but has to be calculated using appropriate codes, e.g. NEMEC [15] for the PS current and DKES [16] or analytic approximations [17] for the bootstrap and inductive currents. The NEMEC equilibrium code is further used to map the spatial co-ordinates of local measurements to effective flux surface radii r. Figure 1(b) shows the contributions to the ι profile for an ECRH discharge at moderate $\beta = p/(B^2/2\mu_0)$. The PS current is of minor importance but the bootstrap current significantly increases ι ('+BS' in figure 1(b)). The usual operation of W7-AS is without net plasma current, $I_p = I_{BS} + I_{OH} = 0$, i.e. the bootstrap current I_{BS} is compensated by an inductive current I_{OH} (profile 'total' in figure 1(b)). This keeps the boundary value ι_a fixed and limits confinement dependent excursions of ι. The local difference in the current densities j_{BS} and j_{OH} of bootstrap and inductive current results in finite but moderate shear, which is largest close to the axis, where j_{BS} vanishes but j_{OH} has its maximum. Large shear, positive as well as negative, can be produced by driving large net currents, e.g. inductively (figure 1(c)). At very high β,

which is achieved with neutral beam heating [18], significant shear is produced by the PS current (figure 1(*d*)).

In the following, only ECRH plasmas at moderate β ($\beta_0 < 1\%$) will be considered. The discharges are centrally heated with perpendicular launch and up to 450 kW ECRH power at 140 or 70 GHz (second harmonic X mode or first harmonic O mode at $B = 2.5$ T). For all conditions, even with inductive currents of up to 30 kA, the ohmic heating power is negligible (<10 kW). The line integrated density is kept fixed by feedback controlled gas puffing. The experimental control parameters are the boundary value of the rotational transform and the net plasma current. For most of the discharges the plasma aperture was narrowed by the limiters such that the effective plasma radius was reduced to $a \approx 0.15$ cm. For optimum confinement conditions the central electron temperature reaches up to $T_e = 2.5$ keV, with the ion temperature $T_i \leqslant 450$ eV being much smaller. For these parameters confinement is governed by electron heat transport and the electrons are energetically decoupled from the ions. Electron heat transport is experimentally assessed from the power balance analysis of T_e profiles obtained from Thomson scattering and ECE measurements. The measurement of global confinement is based on diamagnetic loop data. In cases where temperature and density profiles are available, the electron kinetic energy content W_e is additionally obtained by profile integration.

3. Experiments with current control

Owing to relatively small shear, net current free discharges (figure 1(*b*)) are best suited to probe the dependence of confinement on the value of the rotational transform. They exhibit the most prominent sensitivity to the boundary value ι_a, as is seen from the extensive ι_a scan [6] in figure 2. Narrow regions of optimum confinement exist close to $\iota_a = 1/3$ and $1/2$, where the plasma energy is higher by a factor of about 2 than otherwise. Other, but smaller, maxima exist, for example close to $\iota_a = 2/5$. For the discharges of figure 2 the plasma aperture was not reduced by the limiters, so that for $\iota_a > 0.4$ the effective plasma radius shrinks with increasing ι_a owing to the occurrence of $5/m$ islands at the boundary, in particular those with $m = 9$, 10 and 11. Additionally, the diverting properties of these islands lead to localized plasma flow to unprotected wall areas and cause enhanced influx of impurities [19]. Both effects explain the decrease of the plasma energy towards high values of ι_a.

Figure 3 shows the result of the variation of both ι_a and I_p close to $\iota_a = 1/2$, now with reduced plasma aperture [2]. With $I_p = 0$ the narrow confinement optimum close to $\iota_a = 1/2$ is reproduced. With finite but moderate net current, $I_p = 5$ kA, a narrow window of favourable configurations, $0.47 < \iota_a < 0.49$, exists where confinement even exceeds the optimum at $I_p = 0$. Here the particle confinement is improved to a level that inhibits density control, and n_e increases above the reference level $n_e = 4 \times 10^{19}$ m^{-3}. For these discharges the measured plasma energy as well as the corresponding values which have been scaled to the reference density by the $n^{1/2}$ dependence of the ISS95 scaling are given in figure 3. When the magnetic shear is increased by large currents, the strong dependence of confinement on ι_a is smoothed ($I_p = 15$ kA) and finally lost ($I_p = 25$ kA). Remarkably, with high currents the optimum confinement level is reached for any ι_a, indicating a beneficial role of magnetic shear. Two remarks have to be made with respect to the absolute value of the measured plasma energy. With constant limiter aperture the plasma radius and the length of the interferometer chord, which is used for density control, change with the plasma current. NEMEC calculations and the ISS95 scaling show that for $I_p = 25$ kA this effect contributes only 15% to the improvement in confinement. More importantly, the diamagnetic loop picks up some uncompensated magnetic flux arising from the plasma current. It is assumed that this perturbation does not depend on the particular value of ι_a. The stored plasma energy in figure 3 has therefore been derived from the diamagnetic energy signal by adding a correction, $\Delta W_{dia,Ip}$, which is determined by comparison of W_{dia} and W_e at $\iota_a = 0.51$. For $I_p = 25$ kA

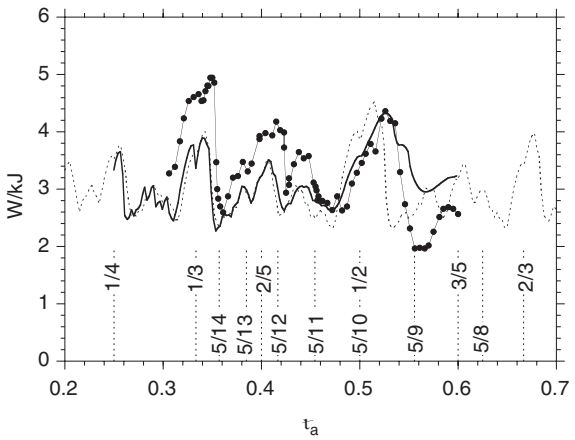

Figure 2. Variation of the plasma energy with the boundary value ι_a of the rotational transform in net current free discharges. Symbols represent the measured diamagnetic energy. In addition, the electron kinetic energy content is shown as calculated from the transport model with the small shear in the vacuum field taken into account (full line) or not (dashed line). $P_{ECRH} = 340$ kW, $n_e \approx 2.3 \times 10^{19}$ m^{-3}.

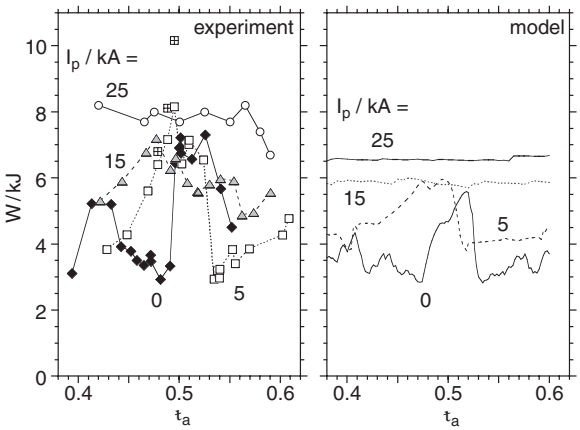

Figure 3. Plasma energy (experiment, derived from diamagnetic loop data) and calculated electron kinetic energy content (model) versus ι_a for various net plasma currents I_p. For three discharges with 5 kA, density control has been lost and the measured energy (crossed squares) has been scaled to the reference density by $n_e^{1/2}$. $P_{ECRH} = 450$ kW, $n_e \approx 4.0 \times 10^{19}$ m^{-3}.

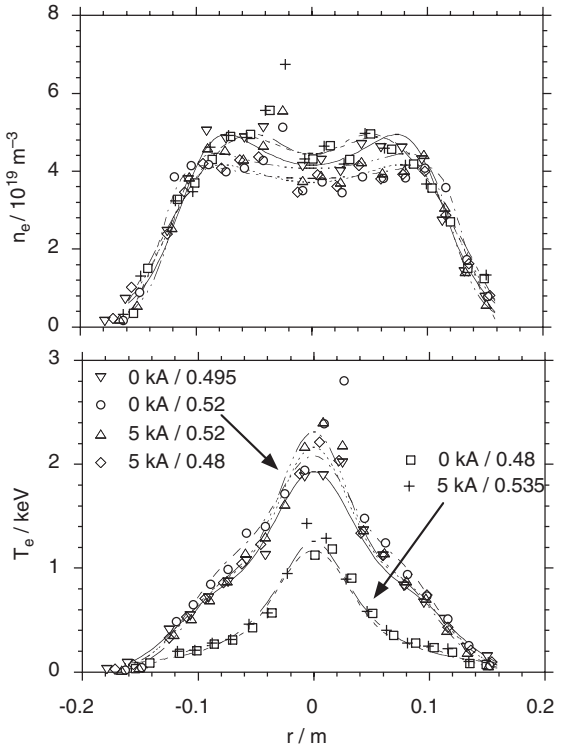

Figure 4. Electron density and temperature profiles for selected discharges of figure 3 at degraded and optimum confinement.

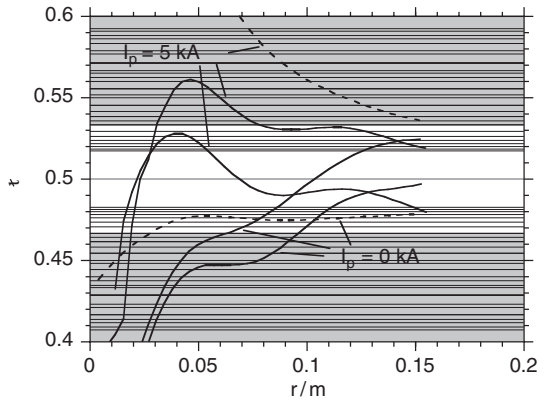

Figure 5. Profiles of the rotational transform for the discharges in figure 4 (full lines: optimum confinement; dashed lines: degraded confinement). The horizontal lines indicate rational values $\iota = n/m$ with $m \leqslant 30$; the shaded area covers the range of $m \leqslant 15$.

the correction is $\Delta W_{dia,Ip} = +2.6\,\mathrm{kJ}$, which is 50% of the diamagnetic loop signal.

Electron density and temperature profiles of some of the low current discharges are given in figure 4. The density profiles appear to be very robust and are similar for all conditions, although changes in particle transport are evident. Previous particle transport studies in W7-AS have concentrated on ι_a values below 0.4, where the particle sources can be better assessed. In stationary regimes near $\iota_a = 1/3$, the particle diffusivity at degraded and optimum confinement has been found to differ by a factor of 2 [20], and we have to expect a similar behaviour close to $\iota_a = 1/2$. Transient changes of the density profile can be observed in dynamic experiments that shift the rotational transform across the critical values where confinement changes, for example by ramping or modulating the plasma current [21]. The observed stiffness of the stationary density profiles is probably due to feedback control of the line integrated density that causes enhanced particle losses to be replaced by enhanced gas puffing. In contrast, the temperature profiles react strongly. Very flat T_e gradients at $r \geqslant 0.05\,\mathrm{m}$ indicate that confinement degradation is caused by enhanced electron energy transport. For optimum confinement a steep T_e gradient extends to the edge. The ι profiles calculated with NEMEC and DKES are shown in figure 5. For reference, the rational values $\iota = n/m$ up to $m = 15$ and up to $m = 30$ are indicated. In the vicinity of the low order rational values $1/2$, $1/3$, etc, the density of such higher order resonances is small. This gap narrows when the maximum m number is increased. Keeping in mind that we do not yet know the maximum relevant m number and that an uncertainty in the experimental ι scale of about 0.005 exists, the following interpretation emerges from the figure: A locally flat T_e gradient, i.e. enhanced transport, correlates with the ι profile having small shear and being simultaneously in a range with densely spaced rational values (case $\iota_a = 0.48$ with $I_p = 0$). In contrast, the T_e gradient is steep, i.e. transport is low, if ι is in the narrow resonance free region (which implies small shear) or if the shear is significant. The latter is always the case close to the centre. Consistently, a central peaking of the temperature profile is observed that is broader than the width of the ECRH deposition zone. The low confinement case, $\iota_a = 0.535$ and $I_p = 5\,\mathrm{kA}$, which has significant shear, seems not to fit into this picture. In spite of reduced aperture, this discharge may additionally be affected by the very strong 5/9 perturbation. The calculated bootstrap current is 2 kA in the low confinement discharges and increases to 7 kA at high confinement. The favourable configurations in figure 3 with $I_p = 5\,\mathrm{kA}$ and $0.47 < \iota_a < 0.49$ require only a small amount of inductive counter current drive, $I_p \approx -2\,\mathrm{kA}$, i.e. the plasma current is nearly self-sustained. These discharges exhibit the particular feature that, except in the very centre, the shear is very low, allowing ι to lie in the resonance free region over a wide radial range. Obviously this leads to very good global confinement.

Plasma current scans with higher resolution have been performed at $\iota_a = 0.51$ and 0.42. The minor plasma radius a was kept constant by adjusting the limiter aperture to compensate for the variation of a with I_p. To avoid the uncertainties of the diamagnetic loop signal at large currents, the electron kinetic energy has been evaluated for each discharge (figure 6). For technical reasons, only positive currents could be applied at $\iota_a = 0.51$ (optimum confinement for $I_p = 0$). Small currents, $I_p \leqslant 3\,\mathrm{kA}$, slightly improve confinement but increasing I_p beyond 5 kA causes a strong deterioration, presumably since the ι profile is shifted with low shear into the range with a high density of rational values. Confinement recovers when shear is increased by higher currents. At $\iota_a = 0.42$ (degraded confinement for $I_p = 0$), negative currents could be applied as well. Here confinement scales nearly monotonically with $|I_p|$ (actually, within the resolution of the scan, the confinement minimum is found at $I_p = +5\,\mathrm{kA}$). This indicates that the anomalous

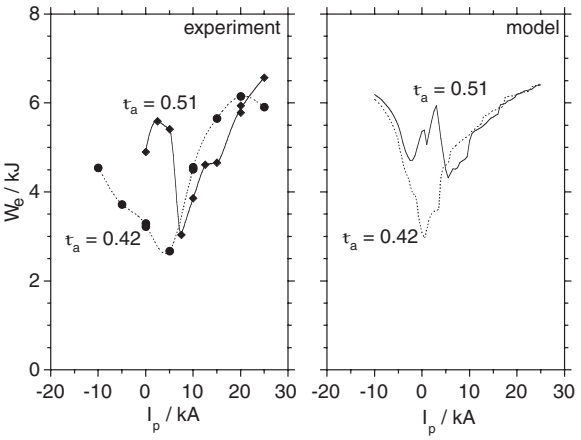

Figure 6. Variation of the electron kinetic energy content (from experiment and model) with the net plasma current I_p at $\iota_a = 0.42$ and 0.51. $P_{ECRH} = 450\,\mathrm{kW}$, $n_e \approx 4.0 \times 10^{19}\ \mathrm{m}^{-3}$.

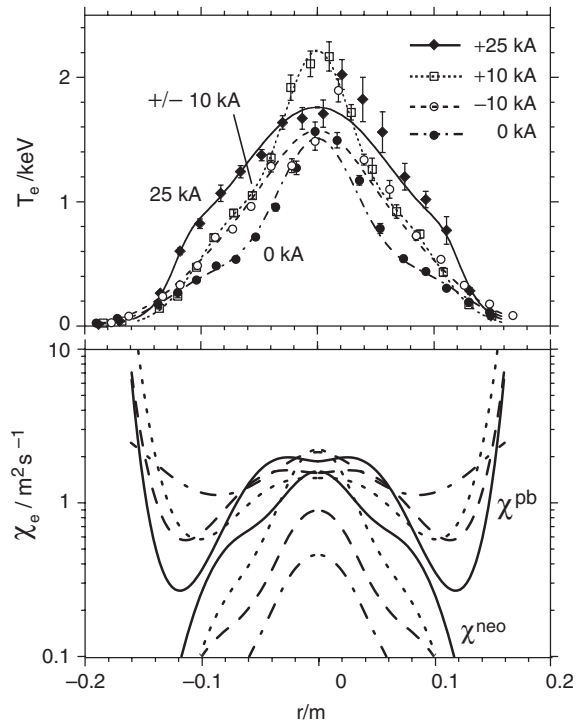

Figure 7. Electron temperature profiles and profiles of the electron heat conductivity derived from power balance and from neoclassical calculations for selected discharges of figure 6 at different plasma currents and $\iota_a = 0.42$.

electron transport does not depend on the sign of the magnetic shear. A similar result was obtained for lower density plasmas [3]. Compared with the degraded situation, $\iota_a = 0.42$ and $I_p = 0$, the temperature gradient strongly steepens with increasing shear at the outer radii (figure 7; the ι profiles for these discharges are those of figure 1(c)). Here the anomalous heat conductivity is strongly reduced by a factor of up to 5 (χ^{pb} in figure 7). In parallel, neoclassical transport (the 'ion root' solution from the DKES code) becomes larger throughout the volume since in the prevailing $1/\nu$ regime the neoclassical heat conductivity increases with $T_e^{7/2}$. Both effects—reduction of anomalous transport and enhanced neoclassical transport at larger temperatures—cause the region that is neoclassically dominated to expand with shear. Towards the boundary, $r > 10\,\mathrm{cm}$, transport remains anomalously high even with high shear.

4. An empirical model of electron energy transport

The experimental results clearly show that in W7-AS a relation exists between anomalous electron transport and both rational values in the rotational transform profile and the magnetic shear. Similar results were previously observed in W VII-A [5], with the difference that the ι_a dependence of confinement vanishes with increasing shear but at a level lower than the optimum. This was interpreted as being due to the overlap of magnetic islands, the latter arising from static external perturbation fields, when shear becomes too large [7]. (It should be noted that the maximum average current density $I_p/(a^2\pi)$, with $I_p \leqslant 4\,\mathrm{kA}$ and $a = 0.10\,\mathrm{m}$, was smaller by a factor of about 2.5 in the W VII-A experiments.)

For several reasons, the dependences found in W7-AS can hardly be explained by island formation at ι values that are in resonance with those components of the external perturbation field spectrum which have been identified by flux surface mapping, i.e. the natural $5/m$ components and the 1/2, 1/3, etc, components from field errors:

- Confinement is also degraded for ι_a values, e.g. 0.48, where nested closed flux surfaces without islands exist in the vacuum field.
- The perturbation amplitudes rapidly decrease towards the magnetic axis. In most of the experiments, however, the plasma radius was reduced by the movable limiters.
- Confinement at $\iota_a = 0.55$ is still degraded when the 5/9 vacuum field islands are compensated by the control coils.
- Large shear would lead to island overlap, which contradicts the good confinement observed.
- A confinement model [6] which short-circuits electron transport across island regions, their width and location being determined from the measured perturbation field spectrum by a field mapping procedure [7], does not reproduce the experimental dependences. This model, however, does not self-consistently account for the coupling of transport and ι profile.

We therefore assume that perturbations at any rational flux surface, produced, for example, by MHD activity or turbulence, can in principle enhance electron energy transport. It is furthermore assumed that, independent of its sign, magnetic shear reduces these perturbations. These ideas are comprised in a simple empirical expression for the electron heat conductivity χ_e:

$$\chi_e(r, \iota, \iota') = \chi_{neo}(r) + \chi_0(r) + \Sigma\chi_{nm}(\iota, \iota'). \qquad (1a)$$

χ_{neo} is the neoclassical electron heat conductivity, which is a lower limit for transport. Owing to its strong $1/\nu$ increase in the long mean free path regime, neoclassical transport in stellarators limits the accessible temperatures, particularly in the centre. Adequate simple analytical expressions for χ_{neo} are not available for W7-AS. For the purpose of modelling we therefore use the simple parameterization

$$\chi_{neo}(r) = \exp[\Sigma b_i (r/a)^i]\ (\mathrm{m}^2/\mathrm{s}) \qquad (1b)$$

which is finite in the centre and accounts for the fast decrease of neoclassical transport towards the boundary. For calculations $b_0 = -0.69$, $b_2 = -10$, any other $b_i = 0$ have been used, which yields $\chi_{neo} = 0.5\ \mathrm{m}^2/\mathrm{s}$ in the centre. Even at optimum confinement conditions, i.e. in the absence of rational values in the ι profile, transport anomalously increases towards the edge. This is accounted for by the term χ_0. A previous regression analysis of the anomalous heat conductivity at optimum confinement conditions in W7-AS showed an inverse scaling of χ_e with the local density and an increase with the global heating power [22]. We adopt this scaling,

$$\chi_0(r) = c_1[n_e(r)/10^{20}\ \mathrm{m}^{-3}]^{c2}(P/\mathrm{MW})^{c3} \qquad (1c)$$

with $c_2 = -1$ and $c_3 = +0.75$. For c_1, which contains the dependence on the magnetic field and the rotational transform, we use $c_1 = 0.45\ \mathrm{m}^2/\mathrm{s}$. This roughly accords with the value $0.52\,\mathrm{m}^2/\mathrm{s}$ from the regression expression [22] for $B = 2.5\,\mathrm{T}$ and $\iota = 0.5$. The first version of the model [21] used equation (1b) for $\chi_0 + \chi_{neo}$ with the need for an additional coefficient to account for the increase towards the edge. The present version reduces the number of model parameters and implies both the empirical density and the power scaling of transport.

The basic point of the model is that, close to a rational surface, $\iota = n/m$, χ_e is additionally increased by

$$\chi_{nm} = \alpha_{nm} \exp(-|\iota - n/m|/\delta - \gamma|\iota'|). \qquad (1d)$$

When moving away from the rational surface, χ_{nm} exponentially decreases with $\iota - n/m$ on the scale δ. Furthermore, the enhancement is exponentially damped with the absolute value of the shear, ι'. In general the amplitudes α_{nm} will depend on the mode numbers m and n. They are expected to become small towards high m since the poloidal scale length of any related perturbations would become small and would not be relevant for transport. Being restricted in m, the density of rational numbers is small close to the low order ones, i.e. there are gaps where transport is low. These gaps correspond to the confinement optima. For simplicity we assume constant amplitudes and introduce an upper limit in the m numbers, $m \leqslant m_{max}$. Furthermore, we assume that a rational surface contributes to the sum only once irrespective of its degeneracy g_{nm}. This means $\alpha_{nm} = \alpha g_{nm}^{-1}$. The constants α, δ, γ and m_{max} have been determined by comparing results from the model with experimental data (see section 5). Reasonable values are $m_{max} = 20$, $\delta = 0.004$, $\gamma = 1.1\,\mathrm{m}$ and $\alpha = 1.1\,\mathrm{m}^2/\mathrm{s}$. Figure 8 shows the variation of $\Sigma\chi_{nm}$ with ι for the shearless case, $\iota' = 0$. $\Sigma\chi_{nm}$ increases the heat conductivity for any ι, except in the neighbourhood of the low order rational values. Therefore good confinement will result if shear is low and ι is placed within such a gap. For reference the electron heat conductivity from the RTP 'q-comb' model [23] is also shown in figure 8. It is noted that a great qualitative similarity exists between the two models.

The ι profile required in equation (1d) is determined from the bootstrap current density j_{BS} and—if a parallel electric field $E_\parallel$ is applied—the inductive current density, $j_{OH} = \sigma E_\parallel$, where σ is the neoclassical electrical conductivity:

$$\iota(r) = \iota_{ex} + \mu_0 R/(Br^2) \int (j_{BS} + j_{OH}) r\ dr. \qquad (2)$$

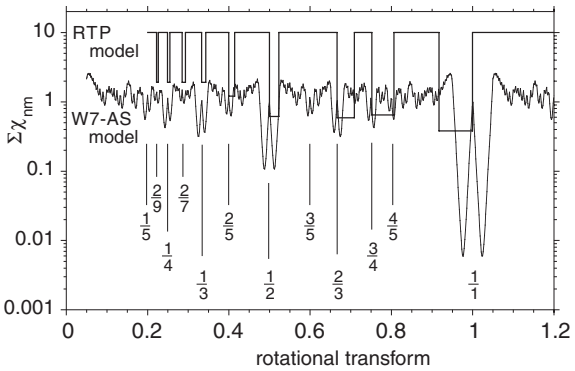

Figure 8. Enhancement $\Sigma\chi_{nm}$ of the anomalous electron heat conductivity at rational surfaces according to equation (1d) of the transport model for $\gamma\iota' = 0$. The position of the low order rational values is indicated. The heat conductivity from the RTP model is shown for comparison.

ι_{ex} is the nearly shearless external rotational transform. PS currents are neglected owing to moderate β and ECRH driven currents are not considered. An accurate treatment of j_{BS} and σ must take into account the full 3-D field structure of W7-AS. This can only be done using large codes, e.g. DKES. However, it has been shown that the bootstrap current behaviour in W7-AS is like that in a tokamak [24]. For simplicity we therefore approximate the bootstrap current density and the electrical conductivity by analytic neoclassical expressions for a tokamak with circular cross-section [17], j_{BS}^{HH} and σ^{HH}, respectively:

$$j_{OH} = \sigma^{HH} E_\parallel \qquad j_{BS} = f_{BS} j_{BS}^{HH}. \qquad (3)$$

The parallel electric field $E_\parallel$ is self-consistently determined from the given net plasma current I_p and the global current balance, $I_p = I_{BS} + I_{OH}$, with $I = 2\pi \int jr\,dr$. The factor f_{BS} accounts for the mean elongation of the W7-AS flux surfaces. A reasonable value has been determined to be in the range $0.5 \leqslant f_{BS} \leqslant 0.7$ by both current balance analysis and a comparison of j_{BS} from equation (3) with DKES calculations (see figure 9). For explicit calculations $f_{BS} = 0.7$ will be used. Given the current densities, and thus $\iota(r)$, the electron heat conductivity can be calculated from equation (1) to obtain the electron temperature profile $T_e(r)$ from the steady state power balance. We use a simplified power balance

$$-4\pi^2 R r n_e \chi_e\ dT_e/dr = P_{heat} \qquad (4)$$

which retains only the heat diffusion term and neglects the heat flux associated with particle flow, radiation losses and electron–ion coupling. $P_{heat}(r)$ is the power deposition profile (heating power deposited within radius r). Relative to the heating power, the radiated power measured by bolometry is below 15% and the estimated power transfer to the ions is 15% for the low and up to 25% for the high confinement discharges considered. In the centre, $r < 10\,\mathrm{cm}$, the diffusive particle flux is negligible because the density profiles are flat. It may become relevant towards the boundary, where n_e and T_e gradient scale lengths are comparable. However, it is neglected for the purpose of modelling. There is no need to postulate a significant heat or particle pinch.

Equations (1)–(4) are strongly coupled since the heat conductivity, being a function of ι, implicitly depends on the

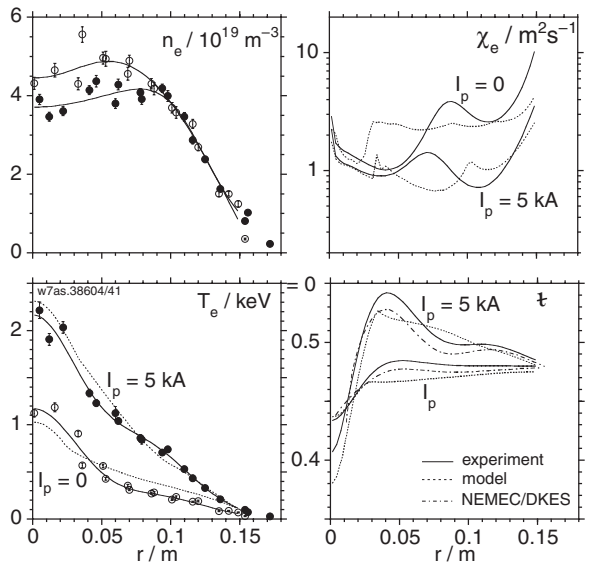

Figure 9. Experimental (data points and full lines, from Thomson scattering) and calculated (dotted lines, from the model) radial profiles of electron density, temperature and heat conductivity and of the rotational transform for discharges with low ($I_p = 0$) and high ($I_p = 5$ kA) confinement at $\iota_a = 0.48$. For comparison the ι profiles calculated by the NEMEC and DKES codes are also given (dashed–dotted lines).

temperature profile via the current densities. Self-consistent solutions for T_e, ι and χ_e are obtained by an iteration procedure which starts with an initial profile for $T_e(r)$. For some conditions, for example when magnetic shear is low and $\iota(r)$ is close to the transition from a resonance free region to a region with densely spaced resonances, convergence of the iteration is poor. Convergence is obtained by a damping algorithm, which uses the weighted average $(y_i + w y_{i-1})/(1 + w)$ with $w \leqslant 4$ of the last two iteration steps as input for the next iteration, where y may be χ_{nm} or j_{BS}. As the criterion for convergence we use that for successive iterations, i and $i + 1$, the average of the relative temperature change, $N^{-1}\Sigma|T_e^i(r_j) - T_e^{i-1}(r_j)|/T_e^i(r_j)$, is smaller than $\varepsilon = 10^{-5}$. The sum runs over the $N = 101$ equidistant radial grid points r_j. The number of iterations typically varies between 30 and 60. In a few cases of poor convergence, only $\varepsilon = 10^{-3}$ is reached after 200 iterations. Density profile (adapted from experiment) and power deposition profile (Gaussian shaped power density with 2 cm HWHM), boundary value ι_a of the rotational transform and, optionally, net plasma current are input to the calculation. For all conditions $Z_{eff} = 2$ and the boundary condition $T_e(a) = 100$ eV are used for the neoclassical calculations and for the integration of equation (4), respectively.

5. Comparison of the model with experimental results

The parameters involved in the χ_e model have been adjusted such that the model calculations reasonably fit the set of discharges from figure 3 with respect to both the T_e profiles and the global confinement, the latter in terms of the volume integrated electron kinetic energy W_e. The calculations have been done for a heating power of $P = 450$ kW and a minor plasma radius of $a = 0.15$ m. Radial profiles for two selected discharges at low ($\iota_a = 0.48$, $I_p = 0$) and high ($\iota_a = 0.48$, $I_p = 5$ kA) confinement are shown in figure 9. The experimental density profiles are used as input to the model. The mean density is $\langle n_e \rangle = 4 \times 10^{19}$ m^{-3}. The calculated temperature profiles reproduce the experimental ones quite well. The ι profiles have been calculated from the tokamak approximations for the current densities, equation (3), using the self-consistent T_e profiles from the model ('model') or the experimental ones ('experiment'), respectively. In both cases the external rotational transform $\iota_{ex}(r)$ is assumed to be radially constant. Additionally, $\iota(r)$ has been calculated using the DKES code for bootstrap and inductive current densities and the NEMEC code for the equilibrium currents. The good agreement between the experimental $\iota(r)$ and the DKES/NEMEC results indicates that the tokamak expressions with appropriate scaling factors reasonably approximate the bootstrap and inductive current densities and that the equilibrium currents are of minor importance for the moderate pressure discharges under consideration with $\beta_0 < 1\%$. Reasonable agreement is also found for the self-consistently determined electron heat conductivity χ_e from the model and the experimental χ_e, which, for consistency, has also been calculated from the simplified power balance, equation (4), using a smooth functional fit to the experimental T_e data prior to differentiation. Both the fitting procedure and the coarse spatial resolution of 2 cm of the T_e diagnostics prevent fine structures which are present in the model χ_e to be resolved experimentally. Towards the boundary we expect χ_e to be overestimated owing to the neglect of the additional loss terms in the power balance.

The observed dependences of global confinement on the boundary value of the rotational transform and the net plasma current are qualitatively reproduced by the model as well. This is shown in figure 3 for the ι_a dependence at selected plasma currents and in figure 6 for the I_p dependence at selected ι_a values. In the case of figure 3 the experimental density profile from the discharge at $\iota_a = 0.495$ and $I_p = 0$ was used in the calculation, in the case of figure 6 that from the discharge at $\iota_a = 0.51$ and $I_p = 0$. Experimental T_e and n_e profiles are not available for all discharges in figure 3, and the calculated electron energy has to be compared with the measured total energy (the same applies to figure 2). The ion temperature can be assessed from the energy spectra of CX neutrals, which yields a line of sight average of T_i. For optimum confinement, e.g. $\iota_a = 0.495$ and $I_p = 0$, $T_i \approx 450$ eV is found, and for degraded confinement, e.g. $\iota_a = 0.48$ and $I_p = 0$, $T_i \approx 280$ eV. Assuming a centrally flat profile form, which is typical for ECRH discharges in W7-AS, we estimate an ion energy content of $W_i = 2.5$ kJ and 1.6 kJ for the respective cases. For optimum confinement, the ion contribution can thus account for the difference between measured total energy and calculated electron energy. For degraded confinement, the model seems to overestimate the electron energy.

With the same χ model parameters but with larger plasma radius, $a = 0.17$ m, reduced heating power, $P = 325$ kW, and reduced density, $\langle n_e \rangle = 2.3 \times 10^{19}$ m^{-3}, conditions which are similar to the experimental conditions of the discharges in figure 2, the profiles for a net current free discharge close to the confinement optimum near $\iota_a = 1/3$ have been calculated.

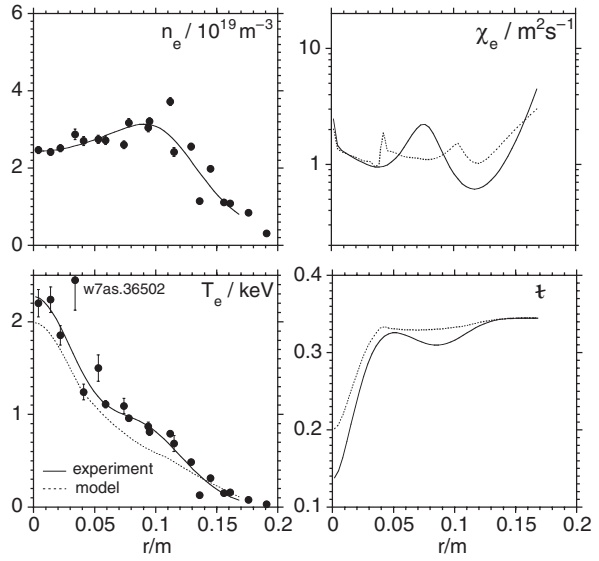

Figure 10. Experimental (from Thomson scattering) and calculated (from the model) radial profiles for a net current free discharge in the confinement optimum at $\iota_a = 0.345$ (conditions as in figure 2).

The model reproduces the experimental T_e profile (figure 10). Using the same input data set, except for the power of $P = 340\,\mathrm{kW}$ adapted to the ι_a scan in figure 2, confinement has been modelled over the full ι_a range for two cases of the external ι profile: (i) $\iota_{ex}(r)$ is assumed to be constant, and (ii) the weak radial variation of $\iota_{ex}(r)$ is taken into account according to figure (*a*). The results are given in figure 2 along with the experimental data. In both cases even fine structures in the experimental ι_a dependence of confinement are reproduced, but the exact position of the maxima is recovered only for case (ii). With constant $\iota_{ex}(r)$ the maxima are centred exactly around the low order rational values. Taking into account the weak vacuum field shear, they are slightly shifted to higher values for $\iota_a > 0.4$ and to lower values for $\iota_a < 0.4$. This corresponds to the experimental findings. When comparing the absolute values of the measured plasma energy and the calculated electron kinetic energy in figure 2, it should be remembered that in the experiment the plasma radius decreases for $\iota_a > 0.4$ owing to the $5/m$ islands, but that a constant value was used in the calculation for the full ι_a range.

The preceding results were obtained for discharges with inductive net current control, i.e. the net plasma current, $I_p = I_{BS} + I_{OH}$, and thus the boundary value of the total rotational transform, $\iota_a = \iota_{ex,a} + \Delta\iota_{Ip}$, are fixed. In this case the iteration procedure converges to a unique solution for any $\iota_{ex,a}$ and I_p, independent of the initial conditions. When the constraint of a fixed net current is relaxed, i.e. $I_{OH} = 0$ and $I_p = I_{BS}$, the current and the total rotational transform self-consistently couple to the confinement and a bifurcation-like phenomenon occurs. Figure 11 shows, for the electron kinetic energy and for the bootstrap current, that in certain windows of the external rotational transform, e.g. $0.38 \leqslant \iota_{ex,a} \leqslant 0.46$, two branches of confinement exist. In other windows, e.g. $0.46 \leqslant \iota_{ex,a} \leqslant 0.52$, only one solution is obtained. The high and low confinement branches are obtained by starting the iteration with a high ($T_{e,0}(r = 0) \geqslant 2.2\,\mathrm{keV}$) and a low ($T_{e,0}(r = 0) \leqslant 0.7\,\mathrm{keV}$) T_e profile, respectively. The form of

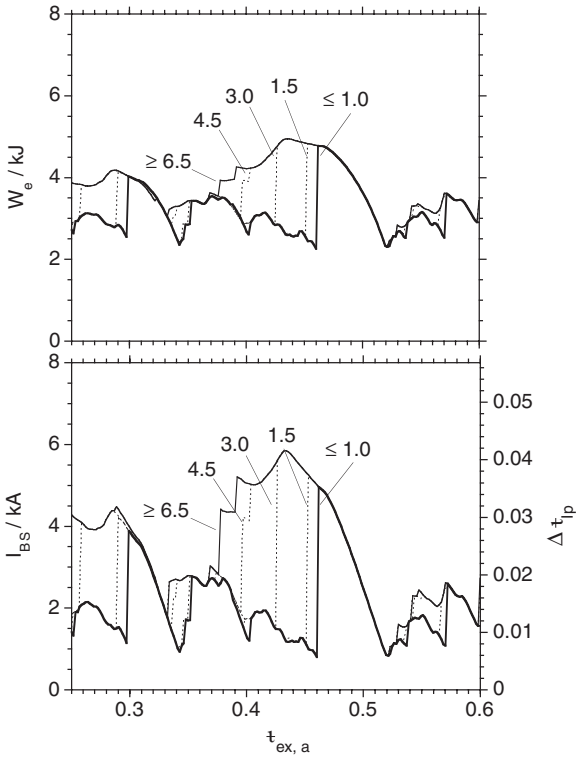

Figure 11. Calculated dependence of electron kinetic energy and bootstrap current on the external rotational transform, where two branches of confinement are predicted if no current control is applied. The curves are labelled by the bootstrap current corresponding to the initial T_e profile for the iteration. $P = 400\,\mathrm{kW}$, $n_e \approx 4.0 \times 10^{19}\ \mathrm{m}^{-3}$, $I_{OH} = 0$.

the profile is the experimental one from the 5 kA discharge in figure 9. For the density the corresponding n_e profile has been used. The curves in figure 11 are labelled by the bootstrap current $I_{BS,0}$ which corresponds to the initial T_e profile. For $I_{BS,0} \leqslant 1.0\,\mathrm{kA}$ the low confinement branch is obtained, for $I_{BS,0} \geqslant 6.5\,\mathrm{kA}$ the high confinement branch. At intermediate currents a transition from the low to the high confinement solution occurs at a $\iota_{ex,a}$ value which decreases with increasing initial current.

High confinement can self-consistently sustain a correspondingly high bootstrap current which produces magnetic shear, thereby reduces transport and—even more importantly—shifts the rotational transform by the amount $\Delta\iota_{Ip}$ from its vacuum field value into the next resonance free region, e.g. around $\iota = 1/2$ ($\Delta\iota_{Ip}$ is indicated on the right hand scale in figure 11). Optimum confinement is therefore predicted for $\iota_{ex,a}$ values well below the next low order rational number, e.g. for 0.43 in figure 11. With low confinement the bootstrap current is not sufficient to drive the rotational transform to the favourable values. For the experiment this implies that a critical initial current must be provided to reach the high confinement branch. This can be achieved, for example, by starting the discharge with external current drive or with a sufficient bootstrap current provided by enhanced heating power.

This prediction was demonstrated experimentally in a sequence of discharges at $\iota_{ex,a} = 0.45$ (figure 12). The plasma current is first ramped to various initial values $I_{p,0}$ by the

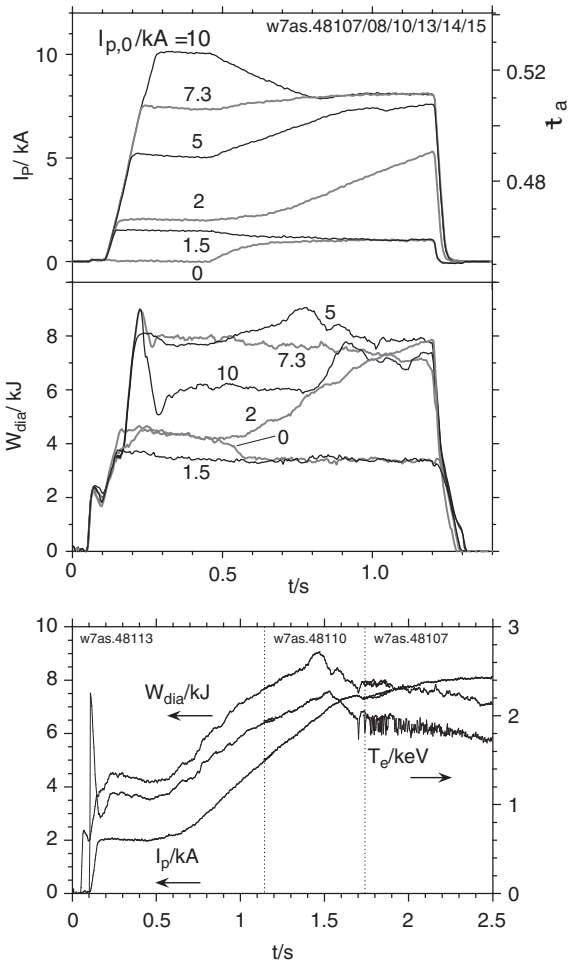

Figure 12. Evolution of plasma current and diamagnetic energy for discharges with initial current control at levels of $I_{p,0}$ and free running current after the external loop voltage is switched off at $t = 0.45$ s. The bottom frame shows the full evolution to high confinement of W_{dia}, I_p and central T_e (from ECE) constructed from the traces of the 2, 5 and 7.3 kA discharges. $P = 400$ kW, $n_e \approx 4.0 \times 10^{19}$ m^{-3}, $t_{ex,a} = 0.45$.

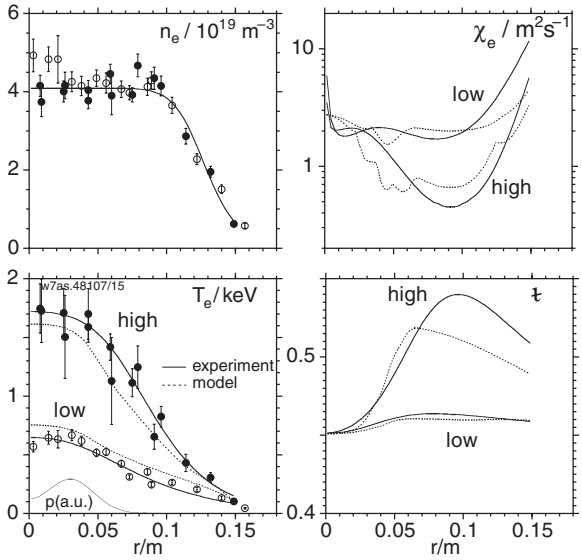

Figure 13. Experimental (from Thomson scattering) and calculated (from the model) radial profiles for the states of low and high confinement which are observed at $t_{ex,a} = 0.45$ in discharges without current control. The Thomson profiles are taken at $t = 1.0$ s from the discharges with $I_{p,0} = 0$ and 7.3 kA in figure 12. The assumed ECRH power density profile p is indicated.

ohmic transformer. After a flat-top phase the external loop voltage is switched off at 0.45 s by keeping the transformer current constant until the end of the discharge, thus allowing the plasma current to evolve freely according to the L/R time and to the temporal changes in confinement. The discharge bifurcates towards low or high confinement at a critical initial current between 1.5 and 2.0 kA. Disregarding the difference between $I_{BS,0}$ and $I_{p,0}$, the initial current for bifurcation is in rough agreement with the prediction of figure 11, where for $I_{BS,0} = 1.5$ kA the transition occurs at $t_{ex,a} = 0.45$ (the damped iteration in the calculation can formally be interpreted as an evolution in time). The stationary high confinement regime is approached within the discharge duration only when the initial current is already close to its stationary value of 8.1 kA, since L/R increases with confinement.

The full evolution from the bifurcation point to high confinement is constructed by shifting the timescale of the discharges at $I_{p,0} = 2$, 5 and 7.3 kA such that their traces continuously match (bottom frame of figure 12). The time for the plasma current to reach steady state is 2.5 s, which can hardly be achieved in W7-AS. The transient confinement optimum at 1.5 s is attributed to a favourable ι profile, as has been discussed in the context of figure 3. After this optimum, confinement tends to become stationary at a somewhat lower level, but stationarity is not really reached. Starting from the centre the temperature slowly decreases in time at a still rising current. This is accompanied by a bursting central mode activity, as can be seen on the central temperature channel from ECE. The activity is located within $r \leqslant 5$ cm and causes temperature variations of up to 250 eV within this radial range. An even m number is deduced from soft X ray and ECE data, and it is probably related to the occurrence of $\iota = 1/2$ at $r \approx 5$ cm (see the ι profile in figure 13). A Δ' code analysis predicts tearing mode instability, which would then be driven by the bootstrap current. The central flattening of the experimental T_e profile could be caused by this mode activity leading to enhanced transport. Instead of introducing an additional enhancement of the central heat conductivity, the discharge is modelled with an off-axis ECRH deposition profile. With a deposition radius of $r_{dep} \approx 3$ cm the experimental and simulated steady state plasma profiles are in rather good agreement for both low and high confinement (figure 13). The experimental ι profile has been obtained after normalizing the bootstrap current calculated from the experimental n_e and T_e profiles (7.2 kA) to the measured plasma current (8.1 kA).

6. Discussion

The experimental dependence of confinement on rotational transform and magnetic shear in ECR heated discharges is rather well described by a simple model which relates anomalous electron energy transport to the presence of rational surfaces. The model is purely phenomenological and does

not make any assumptions about the physical processes involved. In particular, a basic level of anomalous electron energy transport which is present even in the absence of rational surfaces (or at large shear) has to be assumed. This indicates that additional mechanisms are involved in anomalous transport that are not related to rational surfaces.

A particular role is assigned to rational surfaces also by theory. Ideal MHD predicts for a 3-D stellarator equilibrium that the pressure gradient should vanish at a rational surface with $B_{nm} \neq 0$ [25]. Otherwise the parallel current density would be singular. The attempt was not successful to model confinement in W7-AS on the basis of the Fourier components B_{nm} of the static magnetic field spectrum which are known from flux surface mapping [6]. Alternatively, transport at rational surfaces could be enhanced by turbulence or MHD instabilities. Rechester and Rosenbluth [26], for example, have calculated the electron heat conductivity in the case of magnetic field stochasticity, which should arise from magnetic island overlap if microinstabilities are accompanied by magnetic field perturbations of sufficient amplitude. For some cases, fluctuation diagnostics (Mirnov coils, reflectometry and microwave scattering) in W7-AS actually show correlations between the configurational dependence of confinement and the fluctuation pattern. For example, magnetic fluctuations are reduced at the transition from the low to the high confinement states of figure 4 [21], and reflectometry spectra systematically change when confinement improves with magnetic shear [27].

When turbulence is enhanced at rational surfaces, similarities to tokamaks should be expected. Indeed, the global confinement maxima close to low order rational ι in W7-AS strongly resemble the local transport barriers in RTP and other tokamaks at the respective rational q. Since magnetic shear is usually small in W7-AS, any features related to the rotational transform have a large radial extent, i.e. they may become visible in global parameters, whereas they are radially localized in a tokamak with large shear. This would apply in particular to transport if it is related to the local ι value. From this point of view the experimental features of electron transport in W7-AS and RTP appear to be very similar. It is therefore not surprising that the empirical models, which have been independently developed at RTP and W7-AS, have much in common (see figure 8). A basic difference, however, exists in the role of magnetic shear. The damping role of shear observed at W7-AS may be explained by a stabilization of modes or a radial decorrelation of turbulent structures. However, it is not consistent with the tokamak results and the RTP model, which does not have an explicit shear dependence. In the W7-AS model the contributions of rational surfaces to anomalous transport are reduced with increasing shear. Thus the ι gaps of low transport become shallow and finally vanish. Transport barriers are not expected. Experimentally, there is no evidence at W7-AS that the extended ranges of low transport narrow to local barriers when the shear is increased by a plasma current. However, the electron temperature diagnostics that were available in the experiments have only a coarse spatial resolution. Further experiments should reconsider the existence of electron transport barriers in high shear discharges by attempting to increase the resolution of the temperature diagnostics.

The transport model derived from experiments with inductive net current control has also been applied to scenarios without external loop voltage ('true' stellarator operation). The additional degree of freedom leads via the close coupling of transport, bootstrap current and rotational transform to a bifurcation phenomenon with states of low and high confinement for identical external control parameters. The basic features of this prediction were demonstrated experimentally. Apart from giving support to the model, this elucidates once more that, in order to attain experimental control of optimum confinement in stellarators with low vacuum field shear, it is very important to keep the confinement dependent excursions of the boundary value of the rotational transform small. In the standard operation mode of W7-AS this is achieved by inductive net current control, in the optimized W7-X [28] by a strong reduction of both the bootstrap and the Pfirsch–Schlüter current.

References

[1] Sapper J. and Renner H. 1990 *Fusion Technol.* **17** 62
[2] Brakel R. *et al* 1997 *Plasma Phys. Control. Fusion* **39** B273
[3] Erckmann V. *et al* 1997 *Proc. 16th Int. Conf. on Fusion Energy 1996 (Montreal, 1996)* vol 2 (Vienna: IAEA) p 119
[4] Sallander E., Weller A. and W7-AS Team 2000 *Nucl. Fusion* **40** 1499
[5] Grieger G. *et al* 1986 *Plasma Phys. Control. Fusion* **28** 43
[6] Jaenicke R. *et al* 1993 *Nucl. Fusion* **33** 687
[7] Wobig H. *et al* 1987 *Proc. 11th Int. Conf. on Plasma Physics and Controlled Nuclear Fusion Research 1986 (Kyoto, 1986)* vol 2 (Vienna: IAEA) 369
[8] Renner H. *et al* 1992 *Proc. 19th Int. Conf. on Controlled Fusion and Plasma Physics (Innsbruck, 1992)* vol 16C (part I) (Geneva: European Physical Society) p 501
[9] Lopes-Cardozo N. *et al* 1997 *Plasma Phys. Control. Fusion* **39** B303
[10] Schilham A.M.R. *et al* 2001 *Proc. 27th Eur. Conf. on Controlled Fusion and Plasma Physics (Budapest, 2000)* vol 24B (Geneva: European Physical Society) p 1132
[11] Schüller F.C. *et al Proc. 27th Eur. Conf. on Controlled Fusion and Plasma Physics (Budapest, 2000)* vol 24B (Geneva: European Physical Society) p 1697
[12] Stroth U. *et al* 1996 *Nucl. Fusion* **36** 1063
[13] Hirsch M. *et al* 2000 *Plasma Phys. Control. Fusion* **42** A231
[14] McCormick K. *et al* 1999 *Plasma Phys. Control. Fusion* **41** B285
[15] Hirshman S.P., van Rij W.I. and Merkel P. 1986 *Comput. Phys. Commun.* **43** 143
[16] van Rij W.I. and Hirshman S.P. 1989 *Phys. Fluids* B **1** 563
[17] Hinton F.L. and Hazeltine R.D. 1976 *Rev. Mod. Phys.* **48** 239
[18] Kick M. *et al* 1997 *Proc. 16th Int. Conf. on Fusion Energy 1996 (Montreal, 1996)* vol 2 (Vienna: IAEA) p 27
[19] Grigull P. *et al* 1992 *J. Nucl. Mater.* **196–198** 101
[20] Heinrich O. *et al* 1997 *Proc. 24th Eur. Conf. on Controlled Fusion and Plasma Physics (Berchtesgaden, 1997)* vol 21A (Geneva: European Physical Society) p 1593
[21] Brakel R. *et al* 1998 *Proc. 25th Eur. Conf. on Controlled Fusion and Plasma Physics (Prague, 1998)* vol 22C (Geneva: European Physical Society) p 423
[22] Ringler H. *et al* 1990 *Plasma Phys. Control. Fusion* **32** 933
[23] Hogeweij G.M.D. *et al* 1998 *Nucl. Fusion* **38** 1881
[24] Wendland C. *et al* 1999 *Proc. 26th Eur. Conf. on Controlled Fusion and Plasma Physics (Maastricht, 1999)* vol 23J (Geneva: European Physical Society) p 1489
[25] Boozer A.H. 1987 *Encyclopedia of Physical Science and Technology* vol 10 (New York: Academic) p 680
[26] Rechester A.B. and Rosenbluth M.N. 1978 *Phys. Rev. Lett.* **40** 38
[27] Brakel R. *et al* 1998 *J. Plasma Fusion Res.* **1** 80
[28] Grieger G. *et al* 1992 *Phys. Fluids* B **4** 2081